01 Jan 1973

Penetration In Granite By Jets From Shaped-charge Liners Of Six Materials

Ronald R. Rollins
Missouri University of Science and Technology

George Bromley Clark
Missouri University of Science and Technology

H. N. Kalia

Recommended Citation

R. R. Rollins et al., "Penetration In Granite By Jets From Shaped-charge Liners Of Six Materials," *International Journal of Rock Mechanics and Mining Sciences and*, vol. 10, no. 3, Elsevier, Jan 1973.
The definitive version is available at https://doi.org/10.1016/0148-9062(73)90031-4

Int. J. Rock Mech. Min. Sci. & Geomech. Abstr. Vol. 10, pp. 183–207. Pergamon Press 1973. Printed in Great Britain

PENETRATION IN GRANITE BY JETS FROM SHAPED-CHARGE LINERS OF SIX MATERIALS

R. R. ROLLINS and G. B. CLARK

Rock Mechanics & Explosive Research Center, University of Missouri-Rolla, Rolla, Missouri

and

H. N. KALIA

Gates Engineering Co., West Virginia

(*Received* 19 *July* 1972)

Abstract—A new application of theory for three-dimensional collapse of conical liners shows why the two-dimensional analysis may offer a good approximation. Shaped-charge design parameters and rock target properties were investigated to determine their effects on penetration and breakage. Several metals, liner thicknesses, cone angles and standoff ranges for each were investigated. Effective standoff is greater for aluminum than more dense metals. Jets from the 60° monel, brass and steel liners gave the deepest penetration in granite. Jets from copper and brass liners gave equal penetration for 42° apex angles. Liners containing zinc produced small slugs or none at all. The holes in the granite were uniform and approximated right circular cones. Jet penetration velocities into granite varied from a maximum of 10,000 m/sec to a minimum of 2000 m/sec for the most effective metal jet.

NOMENCLATURE

CR	Cone radius
CD	Cone diameter
d	Wall thickness of cone
h	Height of the cone
H_{lim}	Limiting value of charge length
$H.V.$	Hole volume
L	Length of the jet
m	Mass per unit length
m_e	Mass of the liner element
P	Penetration
P_T	Total penetration
P_{max}	Maximum penetration
r_j	Radius of the jet
S	A point between S_2 and S_3
S_2	Normal distance to axis from inner wall of cone
S_3	Normal distance to axis from outer wall of cone
$\dot{S}$	Initial collapse velocity
S_{3i}	Initial value of S_3
SO	Standoff
T	Kinetic energy of collapse
t_1	Jet breakup time
t_c	Collapse time of liner
U_D	Detonation velocity of explosive
U^{min}	Minimum penetration velocity of target
V_j	Jet velocity
V_c	Collapse velocity of liner
V_j^0	Jet-tip velocity
Z_0	Distance from virtual origin (assumed point of origin of jet) to the target surface
α	Half apex angle
β	Collapse angle
γ	$(\rho_t/\rho_j)^{\frac{1}{2}}$
Δl	Length of element along the slant height of cone
λ	Correction factor for discontinuous jet
ρ_t	Density of target
ρ_j	Density of jet

INTRODUCTION

General

THE TERM 'shaped charge' is generally applied to high-explosive cylindrical charges with lined or unlined cavities formed at the end opposite to the point of initiation. The unlined cavity effect is known as the Munroe effect in the United States and the United Kingdom

[1], the Neumann effect in Germany and the cumulation effect in Russia [2]. BAUM [2] has credited Sukhreski with the systematic investigation of the cumulation effect. EICHELBERGER [3] credits R. W. Wood with the recognition in 1936 of the usefulness of metallic liners in the hollow charges to produce fragments of extremely high velocity. Fundamental and developmental studies were simultaneously undertaken by DuPont's Eastern Laboratories, and by Kistiakowsky, Taylor, MacDougal, Jacobs and others in 1941.

This study, undertaken to determine the penetrability of shaped-charge jets into granite utilizing metallic liners and Composition C-4 as the high explosive, was one phase of a broader investigation. While shaped charges have found extensive use in military applications, industrial uses are limited to oil well-casing perforation, furnace tapping, and linear metal cutting charges.

Lined cavity charges have been investigated by CLARK [4], AUSTIN [5] and HUTTLE [6], to evaluate their effect in breaking concrete, rhyolite and limestone boulders. However, no systematic investigation has been made to evaluate shaped charges for drilling and blasting rock. The capability of relatively inexpensive shaped charges to form high-velocity jets makes them of interest for possible application in this operation.

Nature of the Investigation

The primary objective of this study was to evaluate the penetrating capability into rocks of shaped-charge jets produced from liners of selected metals. The following parameters were investigated: (1) property effects of six different liner metals, (2) change in the physical properties of liners by annealing, (3) behavior of rock under jet impact, (4) jet characteristics, formation and penetration theory, and (5) effects of apex angle of conical liners.

A large amount of information is available on the penetration of metallic targets by metallic jets. The first-order penetration law was developed independently by PACK *et al.* [7], PUGH [1] and PACK and EVANS [8, 9] applying Bernoulli's theorem. The total penetration is given by:

$$P = L\,(\rho_j/\rho_t)^{\frac{1}{2}}. \tag{1}$$

Equation (1) holds only for ideal jets and targets with negligible yield strength as compared to the pressure of the jet. Thus, one expects variation from this law for nonideal materials. It is observed that the resistance to penetration in rock is related not only to the density of the jet, its length, and the density of the rock, but to other factors as well, e.g. the joints, bedding planes, porosity and the anisotropic nature of the target.

THEORY OF JET FORMATION AND PENETRATION

The classical two-dimensional theory of jet formation [8, 10] has been modified [3] to account for the jet-tip velocity gradient. The modified two-dimensional theory visualizes the liner collapsing upon itself due to the pressure of the detonation products. As the pressure is applied progressively to the liner, it collapses upon the axis at an angle α (Fig. 1).

The two-dimensional theory and other similar theories neglect the acceleration of the coordinate of the stagnation point and the thickening of the liner. In order to account for these parameters one requires the solution of a three-dimensional time-dependent configuration.

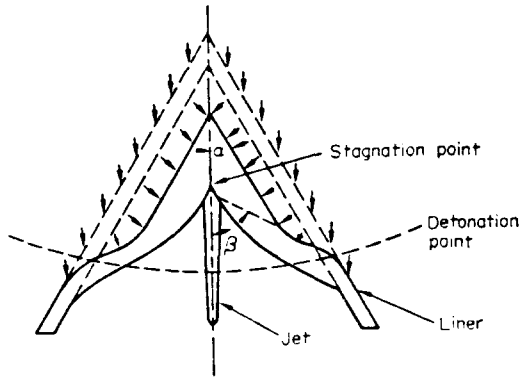

FIG. 1. Cone collapse and jet formation.

Theory of cone collapse and jet formation

The analytical technique used for collapsing cylindrical shells [11] may be applied to collapsing conical liners. When a symmetrical cylindrical shell contracts radially inward with constant kinetic energy the velocity of the outer surface diminishes and the inner velocity increases (Fig. 1). As an initial approximation, it is assumed that the liner material is incompressible and that the wall moves inward normal to the original surface of the cone.

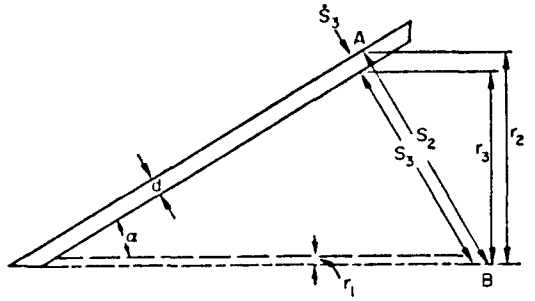

FIG. 2. Cone collapse dimensions.

For a cone of half apex angle α (Fig. 2) the kinetic energy of a thin element of unit thickness can be obtained by considering the section to collapse along the slant height of a cone AB. The kinetic energy of this element is (Appendix A):

$$T = \rho\pi\cos\alpha(S_3\dot{S}_3)^2 \ln S_2/S_3 \tag{2}$$

or the time of collapse is given by

$$t_c = (\rho\pi\Delta l \cos\alpha/T)^{\frac{1}{2}}\, 1/2 \int_{r_1/\cos\alpha}^{S_{3i}} S_3 \ln\left(\frac{S_3 + d}{S_3}\right) dS_3. \tag{3}$$

Equation (3) may be numerically integrated for successive values of S_{3i} and the time of collapse determined for a constant collapse velocity. For a constant jet radius the movement

of the stagnation point is approximately constant (Fig. 3). This partially explains why the two-dimensional theory offers such a good approximation for a three-dimensional process. Modifications of equation (3) similar to those employed by EICHELBERGER [12] and JACKSON [13] for direction and velocity of collapse will yield more accurate evaluation of jet formation.

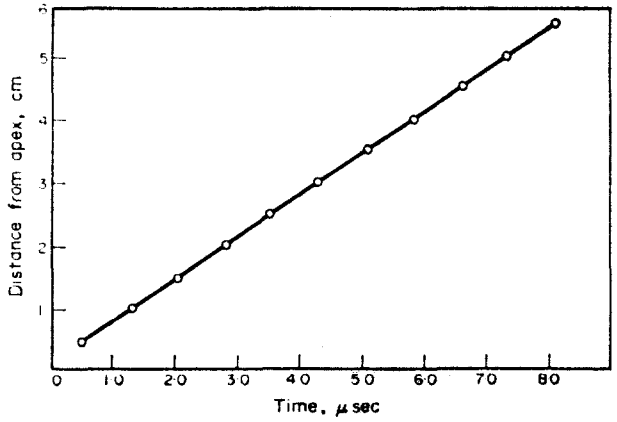

FIG. 3. Collapse time for 60° liners.

Theory of jet penetration

The basic equation for penetration by high-speed metallic jets was developed using Bernoulli's theorem [equation (1)]. Various authors have modified it with empirical constants to explain penetration of various types of metallic targets. DIPERSIO [14] has modified the equations developed by ALLISON and VITALI [15], and the concept of their theory treats three cases: (a) a continuous jet, (b) a partially continuous jet and (c) a completely discontinuous jet. The total penetration for these three conditions is given by

$$P_T = Z_0[V_j^0/(1+\gamma)U^{\min}]^{1/\gamma} \tag{4}$$

$$P_T = \frac{(1+\gamma)(V_j^0 t_1)^{1/(1+\gamma)} Z_0^{\gamma/(1+\gamma)}}{\gamma} - \frac{\sqrt{((1+\gamma)U^{\min} t_1 (V_j^0 t_1)^{1/(1+\gamma)} Z_0^{\gamma/(1+\gamma)})}}{\gamma} - Z_0 \tag{5}$$

$$P_T = \frac{V_j^0 t_1 - \sqrt{(U^{\min} t_1 (V_j^0 t_1 + \gamma Z_0))}}{\gamma}. \tag{6}$$

The basic assumptions used in the development of equations (4)–(6) are that the target and jet are incompressible, the jet originates at a distance Z_0 from the target, the jet breaks up axially into individual particles simultaneously throughout its entire length, and all particles above a critical velocity contribute to penetration in a particular target material.

For a given charge and target the penetration increases linearly with Z_0 for a continuous jet [equation (4)]. The penetration also increases with jet-tip velocity and with a decrease in $U^{\min}$, the minimum penetration velocity, both of which can be determined experimentally. The jet-tip velocity is a function of liner and explosive properties, and $U^{\min}$ a function of the resistance of the target to penetration.

Maximum penetration is obtained at the upper limit of application of equation (6), which defines the penetration for a partially continuous jet:

$$P_{\max} = \sqrt{\left(\frac{\rho_j}{\rho_t}\right)}\left[V_j^0 - \sqrt{\left(U^{\min}\left(V_j^0 + \gamma\frac{Z_0}{t_1}\right)\right)}\right]. \tag{7}$$

That is, maximum penetration is obtained for high jet-tip velocity and optimum jet breakup time, t_1. This equation offers an explanation of the reason that high-velocity explosives and high-density cohesive jets produce a maximum target penetration.

EXPERIMENTAL DESIGN

Design of shaped charges

A summary of shaped-charge design factors affecting penetration in metal is given by KLAMER [16]. For this investigation the following design parameters were considered: (1) liner material, (2) apex angle, (3) liner thickness, (4) charge dimensions and (5) type of explosive, in their effect of penetration into granite.

Liner material. ZERNOW [17] concluded that copper, nickel, aluminum and silver (all face-centered cubic) behave in a similar manner with few noticeable differences between them. They respond in a ductile fashion in the dynamic Bridgman region, and stretch in a taffy-like manner in jet flight. Copper is the most effective liner material for penetrating steel targets, primarily because of its high ductility, low cost and relatively high density.

Iron (body-centered cubic) and all 1020 mild steels also showed high ductility in the dynamic Bridgman region but fractured in relatively large fragments shortly after leaving the high pressure region. The hexagonal metals tested by ZERNOW [17] show distinct characteristics, in flight phase the jets breaking up into fine fragments. Magnesium shows a ductile nature under dynamic pressure while cobalt exhibits an anomalous behavior.

Many metals under higher pressures (21,000–31,500 kg/cm^2) show a different degree of elongation than they do under ambient pressures. The amount of energy consumed in plastic flow and fracturing changes as pressure is increased [18], and hence, the mode of liner failure changes with the applied pressure. Metals having low melting points, such as cadmium (hexagonal), zinc (hexagonal), lead (face centered), and tin (tetragonal), all behave in a unique manner despite the diversity in their crystal structure. It appears that for those metals having melting points $\geqslant$ 625°C the crystal structure correlates with the observed behavior of the jet, whereas for those with very low melting temperatures, 460°C $\leqslant T \leqslant$ 625°C, the low melting point itself appears to be best correlated with the behavior of the jet.

Metals were selected for this investigation (Table 1) with a wide range of physical properties.

Apex angle. Conical liners were used because they are easy to machine and have proved to be one of the most effective geometries. BRIMMER [19] has shown that for metallic targets the optimum cone angle for maximum penetration is approximately 60°, which is the cone angle employed in this study.

TABLE 1. PHYSICAL PROPERTIES OF LINER METALS

Metal type	Tensile strength ($kg/cm^2 \times 10^3$)	Compressive strength ($kg/cm^2 \times 10^3$)	Elongation (%)	Hardness rockwell	Modulus of elasticity ($kg/cm^2 \times 10^5$)	Modulus of rigidity ($kg/cm^2 \times 10^5$)	Metal density (g/cm^3)	Melting point (°C)
Aluminum T-3, 2011	3·866	3·023	15	95E	7·171	2·671	2·82	535–643
Aluminum T-6, 7075	5·835	5·132	17	100E	—	2·742	2·80	476–637
Brass (yellow)	4·288	3·515	23	84K	7·382	2·742	8·47	904·4
Monel	6·679	5·273	27	96B	18·279	6·679	8·84	1300·0
Maraging steel / Vascomax 250	9·8	10·43	19	29C	18·55	7·14	8·0	—
Copper	2·39	—	45–50	34RE	11·95	—	8·96	1083·0

Percentage composition of the metals

Aluminum T-3	Al	93·5%, Cu 5·5%, Pb 0·5%, Bi 0·5%
Aluminum T-6	Al	91·2%, Zn 5·5%, Mg 2·5%, Cu 1·5%, Cr 0·3%
Yellow brass	Cu	65%, Zn 35%
Monel	Ni	66·26%, Cu 31·26%, Fe 1·12%, Al 0·12%, Si 0·7%, C 0·19%, Mn 0·94%
Steel	Ni	18·5%, Co 7·5%, Mo 4·8%, Fe 68·37%, others 0·82%
Copper	Cu	+99%

Liner thickness. The liners were designed with optimum thickness (d_{opt}) which was obtained by using the relationship suggested by WINN [20]:

$$d_{opt} = \frac{d_{opt}(\mathrm{Cu})\,\rho_{Cu}}{\rho_{metal}}. \tag{8}$$

The optimum thickness of the copper liner was taken as 0·105 cm for 60° cones of 5 cm diameter.

The average weights and thickness of the liners are presented in Table 2.

TABLE 2

Metal	Weight (g)	Liner thickness (cm)
Aluminum 2011 (T-3)	32·5 ± 0·25	0·3500 ± 0·002
Aluminum 7075 (T-6)	32·0 ± 0·25	0·3480 ± 0·002
Yellow brass	36·1 ± 0·25	0·1150 ± 0·002
Maraging steel	34·7 ± 0·25	0·1161 ± 0·002
Monel	34·2 ± 0·25	0·1065 ± 0·002
Copper (42°)	47·9 ± 1·00	0·1050 ± 0·002

Dimensions. The charge length must be sufficient to provide a fully developed detonation front before it makes contact with the apex of the liner. BAUM [2] points out that the minimum height of the charge for which its active portion attains a limiting value for a cylindrical charge is equal to $H_{lim} = CR + h$. Thus, H_{lim} for conical liners is approximately equal to 2 cone diameters. Framing camera photographs show that the detonation front for C-4 is fully developed in a length of 2 cone diameters. A standard charge length of 2 cone diameters was used, with a charge to cone diameter ratio of 1·04.

Explosive. Of the characteristics of explosives commonly employed in shaped charges (Table 3), the most desirable properties are high detonation pressure and velocity. Composition C-4 (Table 4) possesses these characteristics and is easy to load by hand. The explosive was loaded at a density of 1·6 g/cm^3 at which it has a theoretical velocity of 8611 m/sec and a detonation pressure of 327,069 kg/cm^2. A mechanical device which applied a controlled pressure was used to ensure uniform loading of the explosive, and a No. 8 blasting cap was adequate for detonation.

Target materials (*Table* 5). Preliminary tests were performed on cast concrete blocks (Table 6) and rhyolite (Table 7). However, these materials were weak and brittle, and it was not possible to obtain hole dimensions. Missouri red granite was used as a standard target material with some tests performed in concrete and rhyolite (Tables 5–7).

EXPERIMENTAL RESULTS

Penetration studies

Penetration depths not including spallation were measured with a graduated metallic probe. Holes were assumed to be right circular cones in shape, and spalled thickness was measured as accurately as possible. The hole was plotted to scale and the slant surface extended to the original rock surface. The radius so obtained was taken as the effective value at the surface.

TABLE 3. SHAPED-CHARGE EXPLOSIVES [19]

Designation	Loading density g/cm³ 25°C	Detonation velocity (m/sec)	Relative power*	Impact sensitivity †	Stability‡	Remarks
Cast Pentolite 50/50	1·65	7500	126	12	Moderately stable	Used chiefly in shaped charges; penetration is 90–95% that of 65/35 Cyclotol. More sensitive than 65/35 Cyclotol.
Cast Cyclotol 65/35	1·71	7995	134	—	Fairly stable	Better for filling small shaped charges
Cyclotol 70/30	1·725	7790	135	14	Fairly stable	One of the most effective shaped-charge explosives; too viscous to load small shaped charges.
Cast RDX	1·65	8180	150	8	Fairly stable	Samples stored 2·5 yr at ordinary temp. found to be perfect. Germans used pressed pre-formed pellets in shaped charges (Comp. A: RDX 90% wax 10%); not used alone in shaped charges.
Cast Comp. B	1·88	7840	133	14	Very stable	About 20% more effective than cast TNT; high shaped-charge efficiency; good loading characteristics; sensitive to shock.
Plastic Comp. C-2 (Dupont)	1·57	7660	126	—	—	Hardens when stored at elevated temperature.
Plastic Comp. C-3	1·60	7625	126	14	Moderately stable	Comp. C modified to provide a good explosive for molded and shaped charges; tends to harden in storage; special packaging needed to prevent exudation even at 55°F.

Plastic C-4	1·59	8578	130	19	Stable	Composition C-4 has been developed to improve the instability and hygroscopy of C-3. Will not undergo exudation at 77°C.
Castable, similar to Comp. B PTX-2	1·70	8065	138	—	Stable	Developed by Picatinny Arsenal as castable filling for shaped sharges.
Small charges pressed; medium and large charges, cast TNT	1·56 cast 1·56 pressed	6640 6825	100	14–15	Very stable	Used for blasting, demolition.
Cast HBX	1·65	7100	113	8	Stable	Intended as replacement for Torpex in depth bombs; generation of hydrogen may deform cavity.
Cast Torpex 2	1·71	7200	116	6	Very stable	Mainly used in underwater ordinance; generation of hydrogen may deform cavity.
Astrolite G Liquid	1·4	8600	174	—	—	Has a very high gas volume. Suitable for shaped charges and fragment acceleration
Astrolite A-1-5 Liquid	1·6	7500	237	—	—	It is a white explosive and melts at 273–280°C. It is very similar to cyclonite in sensitivity, brisance and strength.
Cast HMX	1·84	9124	150	9	—	

* Power of an equal volume of explosive relative to TNT (=100) based on the ballistic mortar.
† Picatinny Arsenal apparatus.
‡ Those classified as moderately stable will survive all but drastic tropical storage; stable and very stable will survive this.

TABLE 4. PROPERTIES OF COMPOSITION C-4

Composition C-4	Percentage	Empirical formula	Heat of formation (kcal/mole)
RDX	91·0	$C_3H_6N_6O_6$	−18·3
Polyisobutylene	2·1	C_4H_8	−19·7‡
Motor oil (SAE 10)	1·6	CH_2	−4·9
Di-(2-ethylhexyl) sebacate	5·3	$C_{26}H_{50}O_4$	−306·9‡
	100·0		
Empirical formula for C-4		$C_{1·80}H_{3·60}N_{2·46}O_{2·50}$	
Heat of formation for C-4		−126·1 kcal/mole	
Heat of reaction for C-4*		983 cal/g	

For this data, a density of 1·59 g/cm³, and the B.K.W. equation of state, the following parameters were computed:†

Density	1·59 g/cm³
Detonation velocity	8578 m/sec
Particle velocity	2320 m/sec
Sound velocity	6258 m/sec
Detonation pressure	312,333 atm
Detonation temperature	3374°K
Total gas	34·667 moles/kg of explosive
Total solid (carbon)	12·176 moles/kg of explosive

* Experimental value from oxygen bomb calorimeter measurements, personal communication from personnel at Picatinny Arsenal.
† Operator's Manual for RUBY, UCRL 6815 or TID 4500.
‡ Personal communication from Dr D. S. Wulfman, UMR [28].

TABLE 5. PHYSICAL PROPERTIES OF TARGET MATERIALS

Rock type	Density (g/cm³)	Impact hardness	Compressive strength (g/cm² × 10⁴)	Compression wave velocity (cm/sec × 10⁵)	Apparent porosity (%)
Concrete	2·069	31*	84·0	4·45*	18·69
Rhyolite	2·620	—	337·0	—	0·16
Missouri Red Granite	2·60	53*	119·0	4·52*	0·4

* Reference [21].

TABLE 6. PENETRATION IN CONCRETE BY 60° LINERS

Charge No.	Liner thickness (cm)	Standoff (cm)	Penetration (cm)
35 S	0·1161	20·0	22·5
36 S	0·1161	15·0	38·5
37 S	0·1161	5·0	31·5
38 S	0·1161	10·0	17·5
49 A16	0·3480	15·0	39·6
50 A 16	0·3480	20·0	22·8
53 A 16	0·3480	15·0	35·5

S—Maraging steel (Vascomax 250).
A16—Aluminum 7075 (T-6).

TABLE 7. PENETRATION IN RHYOLITE BY 60° LINERS

Charge No.	Liner thickness (cm)	Standoff (cm)	Penetration (cm)
42 B	0·115	5·0	10·0
43 B	0·115	10·0	20·0
44 B	0·115	17·5	15·0
45 B	0·115	29·0	22·5
52 A16	0·348	20·0	10·0
54 A16	0·348	15·0	10·0

B—Yellow brass.
A16—Aluminum 7075 (T-6).

An expendable template was designed to centrally locate the detonator and produce a symmetrical detonation front and charges were fired at variable standoff to obtain the optimum value (Table 8). Optimum standoff was also employed in the experiments for measurement of the rate of penetration into granite by jets from liners having 42, 55 and 75° apex angles (Table 9).

TABLE 8. OPTIMUM STANDOFF FOR MAXIMUM PENETRATION

Aluminum 2011 (T-3)	20·0 cm or 4·0 CD
Aluminum 7075 (T-6)	22·5 cm or 4·5 CD
Yellow brass	15·0 cm or 3·0 CD
Monel	17·5 cm or 3·5 CD
Maraging steel	10·0 cm or 2·0 CD
Copper (42°)	16·25 cm or 3·25 CD

Penetration in granite

Aluminum 2011 (*T*-3). Considerable variation in penetration was observed which is attributable to inhomogeneities in the rock and other experimental variables which could not be controlled accurately. Liners with 42, 55 and 75° apex angles produced jets which

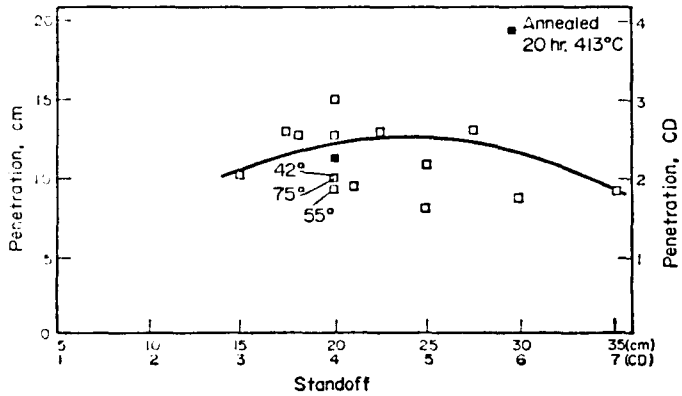

FIG. 4. Penetration in Missouri red granite—60° aluminum 2011 (T-3) liners.

TABLE 9. PENETRATION IN GRANITE—60° LINERS AT OPTIMUM STANDOFF

Charge No.	Apex angle (deg.)	Liner thickness (cm)	Stand off (cm)	Penetration (cm)	Hole radius (cm)	Hole volume (cm^3)
155 T3	42	0·2750	20·0	10·1	—	*
11 T3	55	0·2750	20·0	9·3	3·5	119·3†
57 T3	60	0·3500	20·0	15·0	—	*
154 T3	75	0·3160	20·0	9·9	1·2	14·93
157 T6	42	0·2750	22·5	12·2	0·9	10·35
22 T6	55	0·2750	22·5	11·1	0·5	5·70
G T6	60	0·3480	22·5	13·2	—	—
34 T6	75	0·3160	22·5	9·1	—	—
19 M	42	0·1000	17·5	12·7	1·3	11·3
21 M	55	0·1000	17·5	12·3	0·7	6·3
65 M	60	0·1065	17·5	17·0	1·8	15·6
32 M	75	0·1000	17·5	9·7	0·9	8·2
159 B	42	0·1000	15·0	11·5	1·3	11·3
160 B	55	0·1000	15·0	15·3	0·8	6·3
100 B	60	0·1150	15·0	17·4	1·7	26·2
25 B	75	0·1500	15·0	13·9	0·9	22·5
18 S	42	0·1000	10·0	11·8	0·7	6·0
16 S	55	0·1000	10·0	11·7	1·1	14·8
40 S	60	0·1161	10·0	16·0	1·5	37·7
30 S	75	0·1500	10·0	8·0	0·7	4·1

* Crater (no hole radius could be measured).
† Crater.
T3—Aluminum 2011 (T3).
T6—Aluminum 7075 (T6).
M—Monel.
B—Brass.
S—Steel.
G—From graph.

TABLE 10. PENETRATION IN GRANITE—60° ALUMINUM 2011 (T-3) LINERS

Charge No.	Standoff (cm)	Standoff CD*	Penetration (cm)	Penetration CD*	E.R.† (cm)	H.V.‡ (cm^3)
56	15·0	3·0	10·3	2·06	**	—
60	17·5	3·5	13·0	2·60	2·5	85·1††
62	18·0	3·8	12·8	2·56	**	—
57	20·0	4·0	15·0	3·0	**	—
118	20·0	4·0	12·7	2·54	1·0	13·3
115	21·0	4·2	9·5	1·90	**	—
61	22·5	4·5	13·0	2·60	**	—
59	25·0	5·0	8·0	1·60	**	—
119	25·0	5·0	10·2	2·16	2·5	66·8††
58	27·5	5·5	13·0	2·60	2·0	54·5
116	30·0	6·0	8·8	1·76	**	—
120	35·0	7·0	9·2	1·84	2·0	38·5
A130	20·0	4·0	11·2	2·24	1·2	16·9

* Cone diameters.
† Effective hole radius.
‡ Hole volume.
** Hole was shattered.
†† Conical crater with smooth walls.
A—Annealed liner.

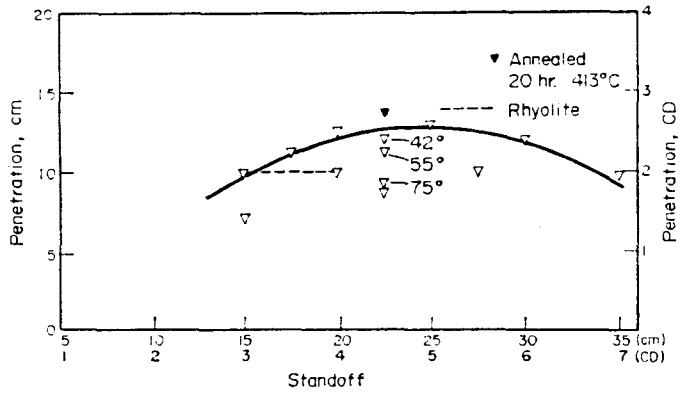

FIG. 5. Penetration in Missouri red granite—60° aluminum 7075 (T-6) liners.

gave less penetration than those from liners with a 60° apex angle. One liner was annealed for 20 hr at 413°C, but this resulted in less penetration. Maximum penetration was obtained at a standoff of 20·0 cm (4·0 cone diameters). (See Fig. 4 and Table 10.)

Aluminum 7075 (*T*-6). A gradual increase in penetration with standoff occurs from 4·0 to 4·5 cone diameters. Jets from 42, 55 and 75° liners when fired at the optimum standoff for 60° liners showed less penetration. One liner which was annealed at 413°C for 20 hr at optimum standoff resulted in a slight increase in penetration. (See Fig. 5 and Table 11.)

TABLE 11. PENETRATION IN GRANITE—60° ALUMINUM 7075 (T-6) LINERS

Charge No.	Standoff (cm)	Standoff CD*	Penetration (cm)	Penetration CD*	E.R.† (cm)	H.V.‡ (cm^3)
54	15·0	3·0	10·0	1·40	1·4	29·3
89	17·5	3·5	11·2	2·24	0·9	8·5
55	20·0	4·0	12·5	2·50	**	—
87	22·5	4·5	8·5	1·70	4·0	142·4††
83	25·0	5·0	13·0	2·60	4·0	217·8††
88	27·5	5·5	10·0	2·00	1·0	11·0
84	32·5	6·5	12·0	2·40	**	—
90	35·0	7·0	9·8	1·96	2·0	41·0††
A131	22·5	4·5	13·7	2·74	0·8	9·2

* Cone diameters.
† Effective hole radius.
‡ Hole volume.
** Hole was shattered.
†† Conical crater with smooth walls.
A—Annealed liner.

Yellow brass. Yellow brass gave greater penetration than all other liners tested. Liners having 42, 55 and 75° apex angles at optimum standoff for the 60° liners gave less penetration than the 60° liners. One of the 60° liners was annealed for 2 hr at 413°C, and gave less penetration than the nonannealed liners. Maximum penetration was obtained at a standoff of 15·0 cm.

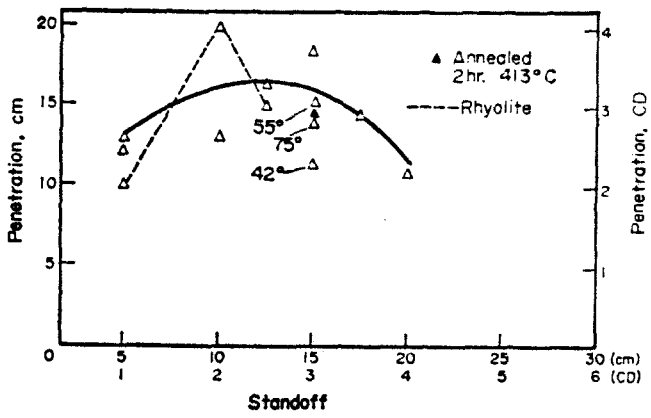

FIG. 6. Penetration in Missouri red granite—60° yellow brass liners.

Three shots were also fired in rhyolite and about 20·0 cm penetration was observed at 10·0 cm standoff. The reliability of the penetration data obtained is questionable due to extensive fracturing of the target, because of the brittle nature of the rhyolite and microfractures present from the quarry blasting. (See Fig. 6 and Table 12.)

TABLE 12. PENETRATION IN GRANITE—60° YELLOW BRASS LINERS

Charge No.	Standoff (cm)	Standoff CD*	Penetration (cm)	Penetration CD*	E.R.† (cm)	H.V.‡ (cm^3)
98	5·0	1·0	13·0	2·6	**	—
99	10·0	2·0	13·0	2·6	1·4	26·7
48	12·5	2·5	16·5	3·3	0·8	11·1
100	15·0	3·0	17·4	3·5	1·7	52·7
103	17·5	3·5	14·5	2·9	1·0	15·2
101	20·0	4·0	10·8	1·2	0·7	5·5
104	5·0	1·0	12·2	2·4	0·7	6·3
A129	15·0	3·0	14·6	2·9	0·8	8·6

* Cone diameters.
† Effective hole radius.
‡ Hole volume.
** Hole was shattered.
A—Annealed liner.

Monel, 60°. Penetration by jets from 42, 55 and 75° liners was less than that for 60° liners. One cone annealed at 871°C for 2 hr gave less penetration than the nonannealed cones. One low value of penetration is attributed to large quartz crystals in the target. The curve is somewhat similar to yellow brass but with less scatter. (See Fig. 7 and Table 13.)

Maraging steel, 60°. The best penetration was obtained at 10·0 cm standoff. The 42, 55 and 75° liners gave less penetration than 60° liners. Since the penetration trend was not promising and this metal required greater machining time, only 3 tests were made. (See Fig. 8 and Table 14.)

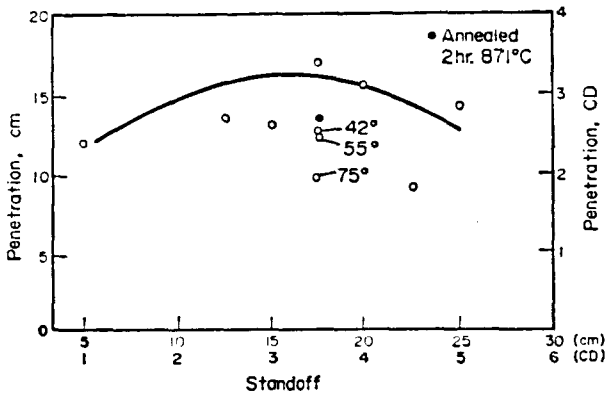

FIG. 7. Penetration in Missouri red granite—60° monel liners.

TABLE 13. PENETRATION IN GRANITE—60° MONEL LINERS

Charge No.	Standoff (cm)	Standoff CD*	Penetration (cm)	Penetration CD*	E.R.† (cm)	H.V.‡ (cm^3)
63	5·0	1·0	12·0	2·4	**	—
64	12·5	2·5	13·5	2·7	1·5	31·8
67	15·0	3·0	13·0	2·6	1·0	13·6
65	17·5	3·5	17·0	3·4	1·8	57·7
66	20·0	4·0	9·0	1·8	4·0	150·8††
68	20·0	4·0	15·5	3·1	**	—
69	25·0	5·0	14·1	2·8	1·0	14·8
A128	17·5	3·5	13·4	2·7	0·9	11·4

* Cone diameters.
† Effective hole radius.
‡ Hole volume.
** Hole was shattered.
†† Smooth-wall conical crater.
A—Annealed liner.

TABLE 14. PENETRATION IN GRANITE—60° MARAGING STEEL (VASCOMAX 250) LINERS

Charge No.	Standoff (cm)	Standoff CD*	Penetration (cm)	Penetration CD*	E.R.† (cm)	H.V.‡ (cm^3)
39	5·0	1·0	14·5	2·90	2·0	60·74††
40	10·0	2·0	16·0	3·20	1·5	37·7
41	15·0	3·0	10·0	2·00	4·0	167·5††

* Cone diameters.
† Effective hole radius.
‡ Hole volume.
†† Smooth-wall conical crater.

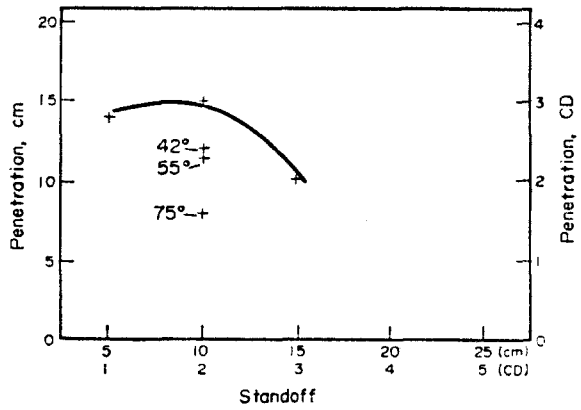

FIG. 8. Penetration in Missouri red granite—60° maraging steel liners.

Copper, 42°. Fifteen jets were fired into granite using 42° copper liners with flanges, and nominal scatter was observed in the penetration data. Flanges were removed from 5 cones, and no significant effects were observed. For this metal, penetration in granite seems to be less sensitive to standoff compared with most other metals. Some of the scatter in data may have been due to the variations in liner mass (46·8–49·5 g) and imperfections in manufacture. (See Fig. 9 and Table 15.)

Summary. The general trend of curves for all the metals is similar (Fig. 10), i.e. an increase in penetration with increase in standoff in accord with theory until a maximum is reached, followed by a decrease in penetration. Charges with aluminum require a greater standoff than those with other metals. This may be due to the cohesiveness of aluminum which is body-centered cubic. All jets have a velocity gradient, with the highest velocity at the tip. All metals but aluminum show maximum penetration at about 2·5–3·5 cone diameters standoff, whereas optimum standoff for aluminum is between 4·0 and 5·0 cone diameters.

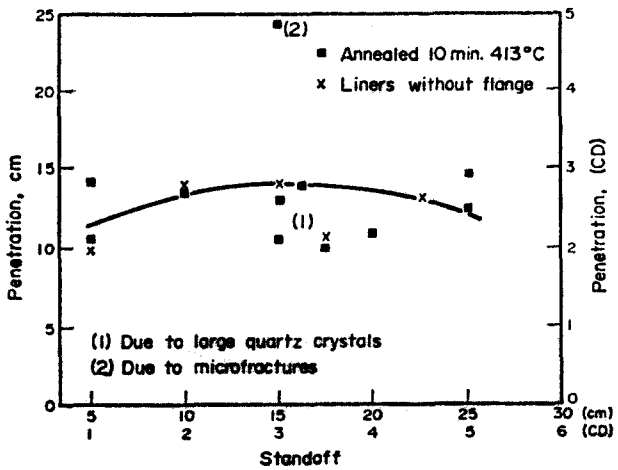

FIG. 9. Penetration in Missouri red granite—42° copper liners.

TABLE 15. PENETRATION IN GRANITE—42° COPPER LINERS

Charge No.	Standoff (cm)	Standoff CD*	Penetration (cm)	Penetration CD*	E.R.† (cm)	H.V.‡ (cm^3)
106	5·0	1·0	14·5	2·90	1·1	18·4
108	10·0	2·0	13·5	2·70	0·9	11·5
107	15·0	3·0	24·5	4·90	1·2	36·9
110	20·0	4·0	11·0	2·20	0·6	4·2
112	15·0	3·0	10·2	2·04		
109	25·0	5·0	12·5	2·50	0·8	8·4
124	5·0	1·0	10·6	2·42	0·9	9·0
125	15·0	3·0	13·2	2·64	0·8	8·8
126	17·5	3·5	10·0	2·00		
128	25·0	5·0	14·8	2·96	0·9	11·2
††145	5·0	1·0	10·0	2·0	1·0	10·5
††146	10·0	2·0	13·6	2·72	1·0	14·2
††147	15·0	3·0	14·3	2·86	1·0	15·0
††148	17·5	3·5	10·8	2·16	1·1	13·7
††149	22·5	4·5	13·2	2·64	1·1	16·7
A127	16·3	3·3	14·1	2·82	0·9	12·0

* Cone diameters.
† Effective hole diameter.
‡ Hole volume.
†† Copper liners without flange.
A—Annealed liner.

Except for aluminum 7075 (T-6) all the annealed liners gave less penetration than non-annealed liners. The scatter in the penetration data was due to the anisotropic nature of the target, variation in liner properties, loading density and other factors.

Although relatively solid, the granite blocks had small joints and the grain structure was nonuniform. Early tests with concrete had shown that joints have a limiting effect on the penetration. The abnormally large penetration observed with copper liner (charge No. 107, penetration 24·5 cm) may have been due to microfractures in the granite from previous testing in the block.

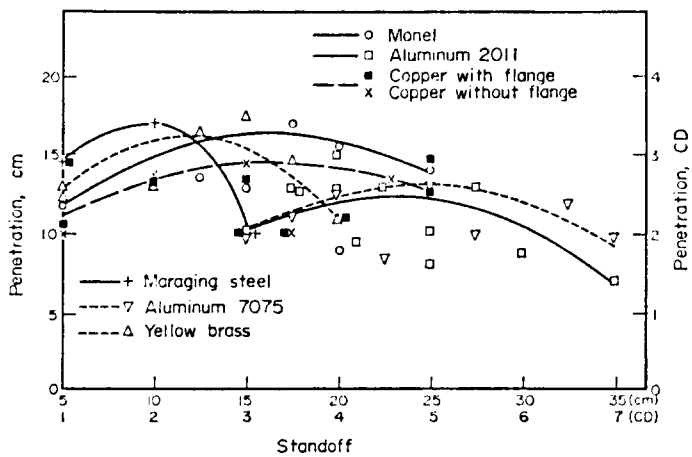

FIG. 10. Penetration in granite—six metals.

Copper jets do not exhibit a superior capability for penetration in granite as they do in steel [19]. The order of effectiveness for penetration in granite is likewise not the same for all metals as in steel, although the steel jets reported by BRIMMER [19] were probably of different material than the steel jets utilized in this study.

Jet characteristics and jet-tip velocity

Attempts were made to photograph jets moving through air and helium atmospheres with a framing camera (Fig. 11). The jet was visible for the first few microseconds, then the interactions between the shock waves created by the jet tip and the atmosphere or the target obscured the jet and the reaction of the target face.

Tests made with flash X-ray equipment by several investigators [2, 18, 25] have shown that jets are continuous and cohesive for a short time. Subsequently the jet breaks up into small particles of approximately the same length. On the basis of published data [14, 15] it is estimated that the jets formed in this investigation remained continuous for the following approximate times:

Aluminum	40–55 μsec
Copper	50–60 μsec
Monel	50–60 μsec
Steel	50–60 μsec
Yellow brass	50–60 μsec

Pin oscilloscope techniques were employed to obtain jet velocities through air and granite. The rate of penetration into granite was obtained by placing pin sets between granite slabs. Two shots per metal were fired to obtain the rate of penetration and jet-tip velocity. The jet-tip velocity through air is given below:

Aluminum 2011 (T-3)	8·09 mm/μsec
Aluminum 7075 (T-6)	7·91 mm/μsec
Copper	8·87 mm/μsec
Monel	9·83 mm/μsec
Steel	7·69 mm/μsec
Yellow brass	8·87 mm/μsec

The velocity decreased rapidly in the first few centimeters (Fig. 12) and then decreased more slowly until maximum penetration (minimum penetration velocity) was reached.

There does not appear to be a direct correlation between either tip velocity or minimum penetration velocity and jet density. The scatter of data may have been due to the inhomogeneity of the rock, erratic performance of probes, or variation in performance of charges.

Penetration involves local shock compression of the materials to very high pressures, possibly accompanied by some local melting and vaporization of the target material. The process of hole enlargement involves extremely high stresses and strains, as well as ejection of material from the hole.

A shock receding into the (continuous) oncoming jet is carried below the original target surface when the jet velocity exceeds the velocity of the shock wave generated in the jet. This critical velocity is a function of the densities and the compressibilities of the jet and target material. As the jet continues to penetrate, the shock wave into the target precedes the jet–target interface. Rarefaction from the free surface of the target and the jet modify the shock system and the shock becomes approximately conical in shape inside the target.

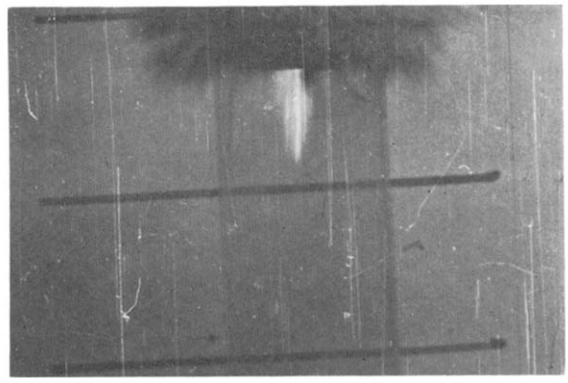

FIG. 11. Shaped charge jet in helium 26 μsec after initiation.

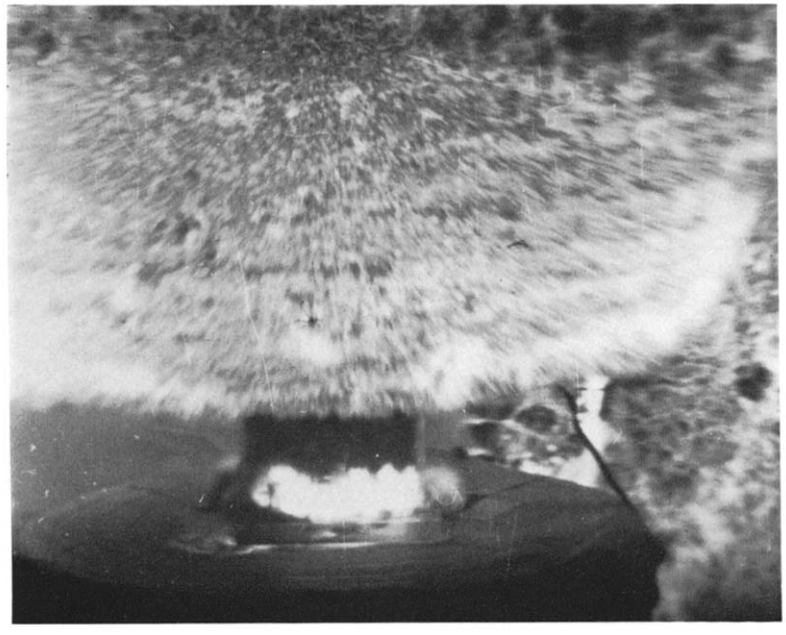

FIG. 13. Detonation front 52 μsec after initiation.

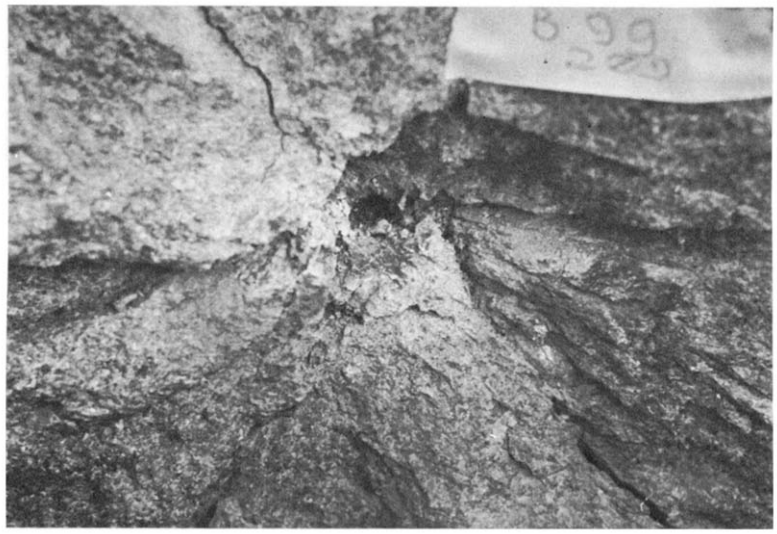

FIG. 14. Fracture pattern in granite.

FIG. 15. Fractures in concrete.

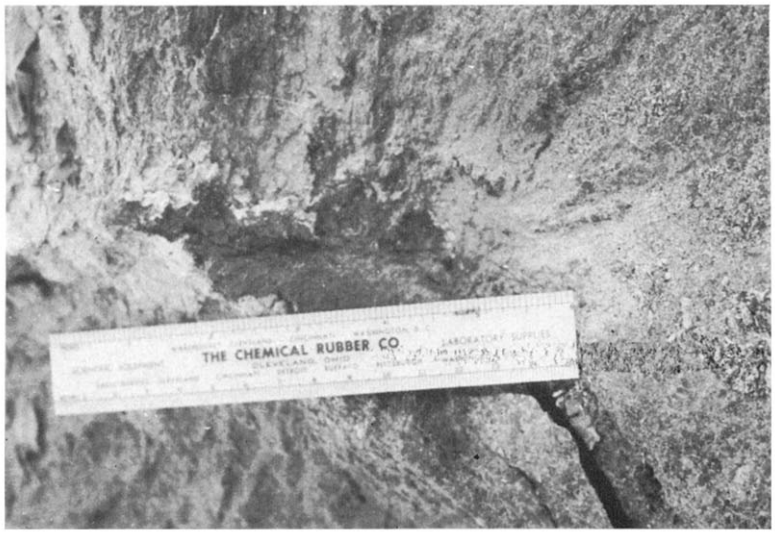

FIG. 16. Longitudinal section of the shaped charge hole.

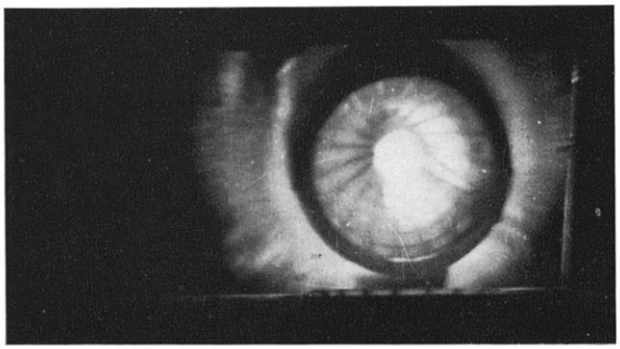

FIG. 17. Interior of collapsing cone.

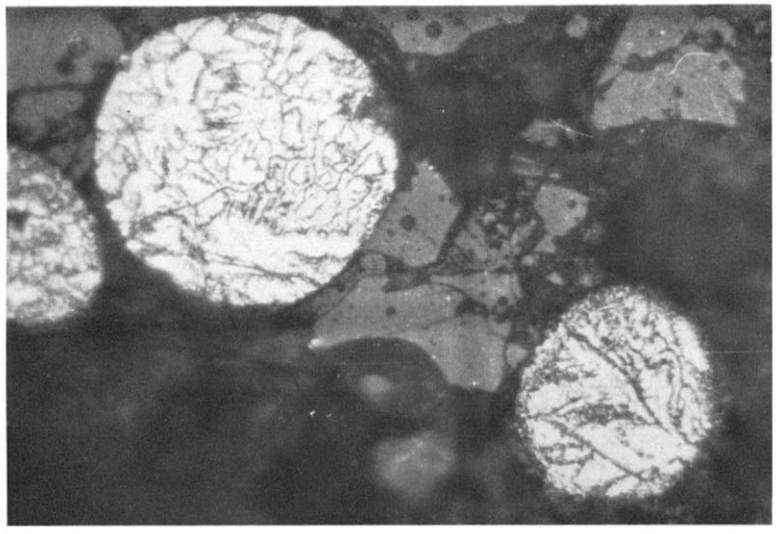

FIG. 18. Photomicrograph of copper imbedded in granite.

FIG. 19. Photomicrograph of steel inclusion of inner wall of a hole in the granite.

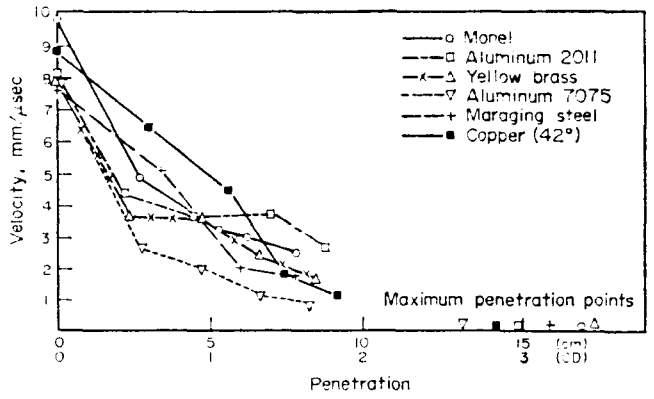

FIG. 12. Jet-tip velocity through granite blocks.

To reduce the probability of shorting out of the pin sets by the shock waves rather than by the jet during rate of penetration measurements the target slab assembly was placed inside a sand-filled container.

Target effects

The manner in which rock behaves under jet impact has not yet been fully explained. BOWDEN [22] has suggested that five different forms of deformation take place in the target material when it is subjected to high-velocity impact pressure by water jets: circumferential surface fractures, subsurface flow and fracture, large-scale plastic deformation leading to permanent deformation, shear deformation around the periphery of the impact zone and failure due to reflection of stress waves.

In general the fractures observed in Missouri red granite were composites of all these types. Attempts were made to observe the development of fractures in the target by the jet. However, the impact of the jet formed a luminous ionized zone (Fig. 13) which obscured both the jet and the target at the point of impact. No fractures in the targets were visible up to 52 μsec after initiation. The fractures described below were developed due to the pressure exerted by the jet on the rock. The major fractures propagate in a radial manner from the hole, suggesting failure due to tension. Also, fracturing continued beyond the jet termination point in concrete blocks.

The pressure at the jet impact point is estimated to be on the order of $1{\cdot}5 \times 10^6$ psi, and diminishes to about one-tenth this value at minimum penetration velocity. However, the duration of pressure at any one point along the axis of penetration is very short. A large portion of the energy is utilized in pulverizing the rock, plastic flow and in transmitting kinetic energy to the ejecta. It is estimated that less than 3 per cent of the kinetic energy of the jet is finally converted to elastic wave energy in the rock. The outgoing wave from the jet hole was strong enough in many cases to cause radial fracturing (Fig. 14). Concrete targets (Fig. 15) also exhibited fracturing beyond the bottom of the jet hole, although some of the fractures may have been caused by waves reflected from the surface of the block. The rapid decrease in pressure effects outward from the axis of the hole is evident in Fig. 16, which shows a zone of pulverization, grading into a zone where the crystals are fractured, and further where the minerals show little microfracturing.

Slug formation and metallographic observations

As a liner begins to collapse due to the detonation pressure the inner wall of the liner moves toward the cone axis at a greater speed than the outer wall. This causes a flow of the liner mass leading to fast jet formation from the inner wall and slow jet or slug formation from the outer wall. The process of cone collapsing was photographed utilizing a mirror with a framing camera. Figure 17 shows the interior of a cone reflected in a mirror with the conical grid, and the development of the flow of the metal. The wall of the liner collapses toward the cone axis forming a solid slug and a jet. However, the latter is not visible.

Slugs from yellow brass cones were smaller than those of other metals, and slugs were recovered from Aluminum 7075. A carefully designed experiment was implemented to collect slugs from aluminum liners, and one slug was obtained from Aluminum 2011. It is suggested that zinc in the alloy is responsible for small slugs, or for the lack of slug formation. Metallography studies were performed on the slugs and metals (Appendix B), and the following conclusions were drawn from studies of the metallographs:

(1) In all cases the grains are elongated and orientated along the direction of the slug's longitudinal axis.
(2) The grains in the slug are smaller than those in metal. In all cases the size of the grains had reduced at least by a factor of ten.
(3) The grain size is smallest near the axis of the slug and increases toward the edge.
(4) In all of the slugs a pin hole or fracture was observed along the longitudinal axis.
(5) For copper and possibly aluminum some evidence of melting of the jet was present. Material from the bottom of the target hole was analyzed microscopically. This revealed spherical inclusions indicating possible melting of copper particles (Fig. 18).
(6) There was indication of recrystallization and twinning in minerals in the granite.
(7) The hardness of the slugs of Aluminum 2011 and brass was less than the undeformed metal, suggesting an annealing effect. In monel and steel the hardness increased, suggesting a small degree of precipitation. However, no evidence of the precipitation was visible in the photomicrographs.
(8) There was no significant change in the densities of the metal in slug formation.

Jet hole characteristics

A high degree of comminution occurred in the material immediately around the hole, where the rock was crushed and friable. Spallation always occurred around the collar of the hole, probably due to rebound, and the granite was highly fractured with metal inclusions in the cracks (Fig. 19).

All of the holes were coated with jet material, each having a coloration characteristic of the liner metal. For brass the holes were brick red while for copper the holes were red. Aluminum, monel and steel gave a black coloration.

In all cases some metal from the jet was deposited at the bottom of the holes in a fan shape. Four types of craters were formed (Fig. 20). Type (d) had very smooth walls which were discolored by carbon from the explosive. As indicated above, some of the holes contained spherical globules indicating melting. However, except for one case (Fig. 18) melting was not evidenced by optical microscopy. In some instances there was evidence of jet material intruding into cracks in the rock.

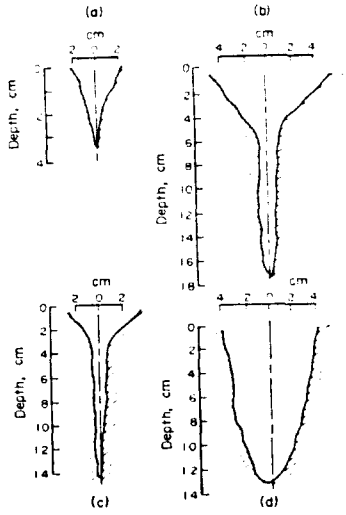

FIG. 20. Typical hole profiles in granite.

SUMMARY AND CONCLUSIONS

Jets from the 60° monel, brass and steel liners gave the deepest penetration. Monel required greater standoff than brass and steel, but less than aluminum. Copper and brass liners gave equal penetration for 42° apex angles. Aluminum liners were easier to machine than other metals. Maraging steel and the monel liners were the most difficult to fabricate. Except for Aluminum 7075 it appears that annealing has no effect on penetration in granite. Aluminum 7075 jets gave a somewhat greater penetration than Aluminum 2011. Liners containing zinc produced small slugs or none at all. The holes in the granite were uniform and approximated right circular cones. About 3–4 cm of the hole was removed by spalling and blast effects for 1·5 in. diameter charges. Fractures in granite due to the jet and blast were caused by compression, tension and shear failure. Rock in the direct line of the jet was highly crushed and powdered, and the jet material had intruded into fractures in the rock.

Jet penetration velocities into granite varied from a maximum of 10,000 m/sec to a minimum of 2000 m/sec for the most effective metal jet. The minimum penetration velocity of all jets was approximately the same for all jets. Metallographic studies indicated a symmetrical liner collapse. Grains were highly fractured and hardness decreased in brass and aluminum, and a phase transition was suspected in steel liners. The density of the slugs was the same as the undeformed metal.

Acknowledgments—This investigation was conducted for DuPont DeNemours Company, Inc., Wilmington, Delaware and Corps of Engineers, Missouri River Division, Omaha, Nebraska, Contract No. DACA-45-69-C-0087.

REFERENCES

1. BIRKHOFF G., MACDOUGAL D. P., PUGH E. M. and Sir TAYLOR G. Explosives with lined cavities. *J. appl. Phys.* **19**, 563–582 (1948).
2. BAUM F. A., STANYKOVICH R. P. and SHEKTER B. I. *Physics of an Explosion* (AD 400 151), p. 546, Research Information Service, New York (1949).
3. EICHELBERGER R. J. *Re-Examination of the Theories of Jet Formation and Target Penetration by Lined Cavity Charges*, Ph.D. Dissertation, Carnegie Institute of Technology, Pittsburgh (1954).

4. CLARK G. B. *Studies of the Design of Shaped Charges and Their Effect in Breaking Concrete Blocks*, A.I.M.E. Technical Paper 2157 (1947).
5. AUSTIN F. C. *Lined-Cavity Charges and Their Use in Rock and Earth Materials*, New Mexico Institute of Technology, Bull. 69 (1959).
6. HUTTL J. B. The shaped charge for cheaper mine blasting. *Engng Min. J.* **147**, 58–63 (1946).
7. HILL R., MOTT H. F. and PACK D. C. *Penetration by Munroe Jets*, Ministry of Supply, A.C. No. 5756, HMSO, London, January (1944).
8. PACK D. C. and EVANS W. M. Penetration by high velocity Munroe Jets—I. *Proc. phys. Soc.* Sect. B **64**, 298–302 (1951).
9. PACK D. C. and EVANS W. M. Penetration by high velocity Munroe Jets—II. *Proc. phys. Soc.* Sect. B **64**, 303 (1951).
10. PUGH E. M., EICHELBERGER R. J. and ROSTOKER N. Theory of jet formation by charges with lined conical cavities. *J. appl. Phys.* **23**, 532–536 (1952).
11. STERNE T. E. A note on collapsing cylindrical shells. *J. appl. Phys.* **21**, 73–74 (1950).
12. EICHELBERGER R. J. Prediction of Shaped Charge Performance from Release Wave Theory, *Transactions of the Symposium on Shaped Charges*, Report BRL 909 (AD 58 899), p. 192, Aberdeen Proving Grounds Maryland (1953).
13. JACKSON R. F. The Problem of Lagrange for Shaped Charge Liner Collapse. *Transactions of the Symposium on Shaped Charges*, Report BRL 909 (AD 58 899), p. 131, Aberdeen Proving Grounds Maryland (1953).
14. DIPERSIO R., SIMON J. and MERENDINO A. B. *Penetration of Shaped Charge Jet into Metallic Targets*, Report BRL 1296 (AD 476 717), Aberdeen Proving Grounds Maryland (1965).
15. ALLISON F. E. and VITALI R. *A New Method of Computing Penetration Variables by Shaped Charge Jets*, Report BRL 1184 (AD 400 485), Aberdeen Proving Grounds Maryland (1963).
16. KLAMER O. A. *Shaped Charge Scaling*, Report AD 600 273 Picatinny Arsenal, Dover, N.J. (1964).
17. ZERNOW L. and SIMON J. High Strain Plasticity of Liner Metals and Jet Behavior, *Transactions of the Symposium on Shaped Charges*, Report BRL 909 (AD 58 899), pp. 107–130, Aberdeen Proving Grounds Maryland (1953).
18. RINEHART J. S. and PEARSON J. *Behavior of Metals Under Impulse Loads*, p. 203, Dover Pubns, New York (1965).
19. BRIMMER R. A. *Manual for Shaped Charge Design*, Navord Report 1248 (ATI 84 949), China Lake, Calif. (1950).
20. WINN H. The Present Status of the Artillery Ammunition Program at the Firestone Tire and Rubber Company, *Transactions of the Symposium on Shaped Charges*, p. 25. Report BRL 909 (AD 58 899), Aberdeen Proving Grounds Maryland (1953).
21. BROWN J. Personal communication (1970).
22. BOWDEN F. P., BRUNTON J. H. The deformation of solids by liquid impact at supersonic speeds. *Proc. R. Soc.* Ser. A **263**, 433 (1961).
23. E. I. DUPONT and Co. *Investigation of Cavity Effect*, Final Report E. I. Dupont de Nemours and Co., Wilmington, Delaware (1943).
24. E. I. DUPONT and Co. *Evaluation of Deep Drawing Steels for Manufacture of Purity Charge Cones*, E. I. Dupont De Nemours and Co. Wilmington, Delaware (1944).
25. CLARK J. C. Flash radiography applied to ordinance problems. *J. appl. Phys.* **20**, 363–370 (1949).
26. ORAVA R. N. and OTTO H. E. The effect of high energy rate forming on terminal characteristics of metal —A review. *J. Metals* 17–30 February (1970).
27. KEHL G. H. *Principles of Metallographic Laboratory Practice*, 3rd edn, McGraw-Hill, New York (1944).
28. WULFMAN D. S. Personal communication (1970).

APPENDIX A

Collapse Time and Kinetic Energy

The following assumptions were used in the development of the expressions presented in the text to obtain liner collapse time and the kinetic energy of collapse:

(1) Metal under high pressure and impulsive load is considered to be an incompressible fluid.
(2) Collapse is normal to the original slant height of the liner.
(3) The initial collapse velocity is constant over the surface of the cone.

Consider a section of the cone and an element on the surface having a small length along the slant height of the cone to be Δl (Fig. 2), thus

$$r_2 = S_2 \cos \alpha$$

$$r_3 = S_3 \cos \alpha$$

and the volume of this element

$$V_e = \tfrac{1}{2}\Delta l \rho \pi \cos (S_2^2 - S_3^2). \tag{A.1}$$

If the volume of the element remains constant then

$$V_e = \text{const.}$$

and therefore

$$(2Ve/\rho \pi \cos\alpha \Delta l) = (S_2^2 - S_3^2)$$

will be conserved as the liner is collapsing. Differentiating $(S_2^2 - S_3^2)$ with respect to time

$$2S_2\dot{S}_2 = 2S_3\dot{S}_3 = 2S\dot{S}$$

for any value of S, thus

$$\dot{S}_3 = (S\,\dot{S}/S_3). \tag{A.2}$$

The kinetic energy (T) of the element is given by

$$T = \tfrac{1}{2}\Delta l \rho \int_0^{2\pi\cos\alpha} \int_{S_3}^{S_2} \mathrm{d}\theta S\,\mathrm{d}S\,(\mathrm{d}S/\mathrm{d}t)^2$$

$$= \Delta l \rho \pi \cos\alpha \int_{S_3}^{S_2} S\,(S\,\mathrm{d}S/\mathrm{d}t)^2\, 1/(S^2)\,\mathrm{d}S$$

$$= \Delta l \rho \pi \cos\alpha\,(S_3\dot{S}_3)^2 \int_{S_3}^{S_2} (1/S)\,\mathrm{d}S$$

$$T = \Delta l \rho \pi \cos\alpha\,(S_3\dot{S}_3)^2 \ln (S_2/S_3). \tag{A.3}$$

From equation (3) $\dot{S}_3$ is given by

$$[\mathrm{d}S_3/\mathrm{d}t]^2 = (\dot{S}_3)^2 = \left[\frac{T}{\Delta l \rho \pi \cos\alpha S_3^2 \ln S_2/S_3}\right].$$

Therefore

$$\mathrm{d}t = \left[\frac{\Delta l \rho \pi \cos\alpha S_3^2 \ln S_2/S_3}{T}\right]^{\frac{1}{2}} \mathrm{d}S_3. \tag{A.4}$$

Integrating equation (4) for t gives

$$\int_0^t \mathrm{d}t = (\rho\pi\Delta l\cos\alpha/T)^{\frac{1}{2}} \int_{r_j}^{S_{3t}} S_3\,(\ln S_2/S_3)^{\frac{1}{2}}\,\mathrm{d}S_3.$$

Therefore

$$t_c = (\rho\pi\Delta l\cos\alpha/T)^{\frac{1}{2}}\, 1/2 \int_{r_j/\cos\alpha}^{S_{3t}} S_3 \ln\left(\frac{S_3 + d}{S_3}\right) \mathrm{d}S_3.$$

APPENDIX B

Metallography of the Metals and Slugs

A systematic metallographic investigation was made to observe the effect of detonation pressure on the shaped-charge liners. Changes in the microstructure following explosive impact and flow are primarily in the distribution density of lattice defects such as dislocations, vacancies, interstitials, stacking faults, mechanical twins and an amount of strain-induced transformation in alloys normally susceptible to such transitions [26]. Pressure imparted to the liners causes a severe deformation and reduction in size of the grains.

A representative sample was taken from the original metals used to fabricate the cones. Samples were prepared for metallographic analysis employing standard procedures [27].

The slugs were cut in a manner to reveal the structure along the longitudinal and the transverse axes. The greatest deformation was near the center of the slug. The grains showed an elongation in the direction towards the stagnation point.

Figure B.1. Aluminum 2011 (T-3). This alloy has a face-centered cubic lattice structure and is free machining. Grain boundaries are well defined and are equiaxed.

Figure B.2. Aluminum 2011 slug. The grains are highly fractured and are about 1/150th of the original grain size. Some recrystallization is indicated. Fine grains are almost equiaxed. A fracture was seen along the transverse axis of the slug near the stagnation axis. The hardness of the metal had decreased from 63 RB to 21 RB.

Figure B.3. Aluminum 7075 (T-6) aluminum zinc alloy. No slug was recovered in this case. The α-grains are well defined and are equiaxed. Mostly α-grains with some black inclusions and boundary precipitation also evident.

Figure B.4. Yellow brass. The α-grains are white and occupy about 90 percent of the area of the specimen. The grains are well defined and are equiaxed.

Figure B.5. Brass slug at the longitudinal axis near the edge of the slug. The grains are fractured and show elongation along the slug axis. The β-particles had elongated near the center of the slug and were highly fractured. The flow of the particles was along the transverse axis of the slug. The hardness had decreased from 73 RB to 53 RB suggesting some annealing effects.

Figures B.6, B.7 and 18. Copper metal, slug and photomicrograph of a copper particle imbedded in granite. In Fig. B.6 annealing twins are visible. The grains are well defined and are equiaxed. Figure B.7 shows the structure of the slug along the longitudinal axis of the slug. No fractures were visible but a pin hole was observed at the center of the slug. The grains are well defined and are equiaxed. The size of the grains is about 1/10th of the original grains. Grains are elongated along the direction of flow. No melting was observed. The grains are completely crushed. Recrystallization after deformation is apparent. Figure 18 is a photomicrograph of the metal particles and highly fractured granite from the end of the hole. Some melting of the metal is evidenced. The hardness of the slug had increased from 34 RE to 14·5 RB.

Figure B.8. Monel metal which shows a roughly equiaxed grain of β-phase containing annealing twins and no second phase. Small amounts of an unidentified second phase inclusion are seen.

Figures B.9, B.10 and B.11. Figure B.9 is a monel slug at the longitudinal axis. The grains are highly deformed and have elongated along the direction of flow. Deformations and flow patterns are clearly visible. Black inclusions of a second phase are lenticular in shape. Figure B.10 shows the structure of the slug at the center. The stagnation point has a large crack and small fractures in a radial pattern. The crack at the center is surrounded by very fine recrystallized grains, several orders of magnitude smaller than the original grains,

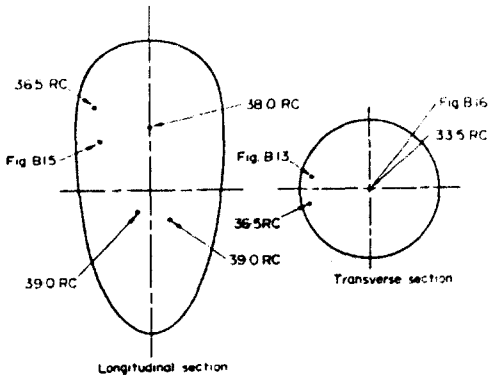

FIG. B.14. Maraging steel slug and hardness.

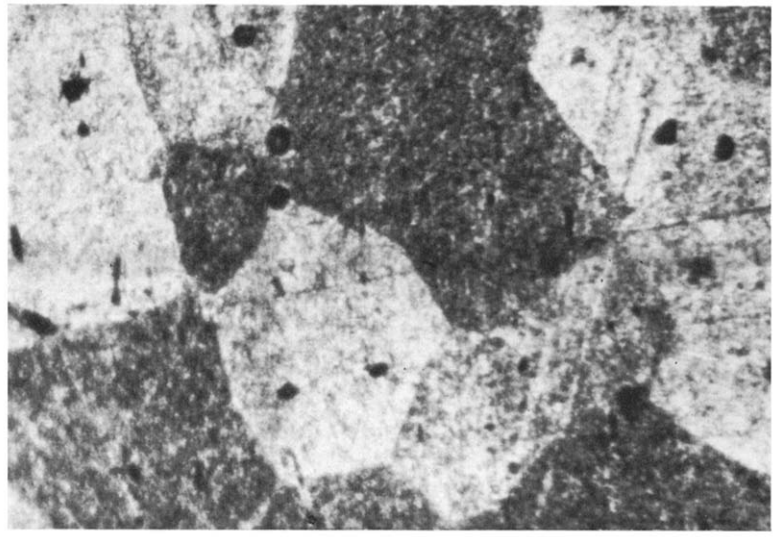

FIG. B.1. Aluminum 2011. × 250

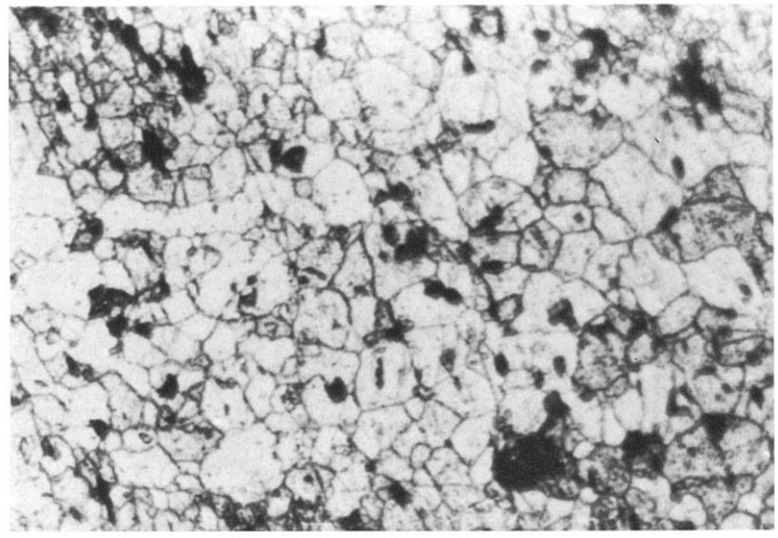

FIG. B.2. Aluminum 2011 slug. × 250

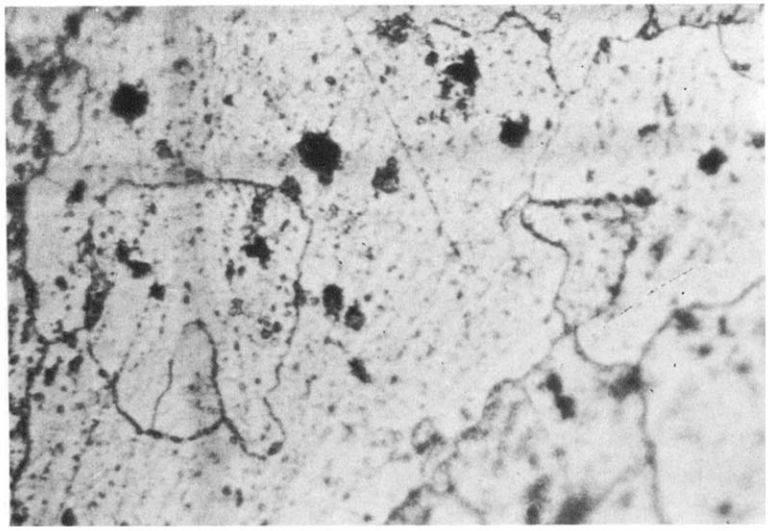

FIG. B.3. Aluminum 7075. × 250

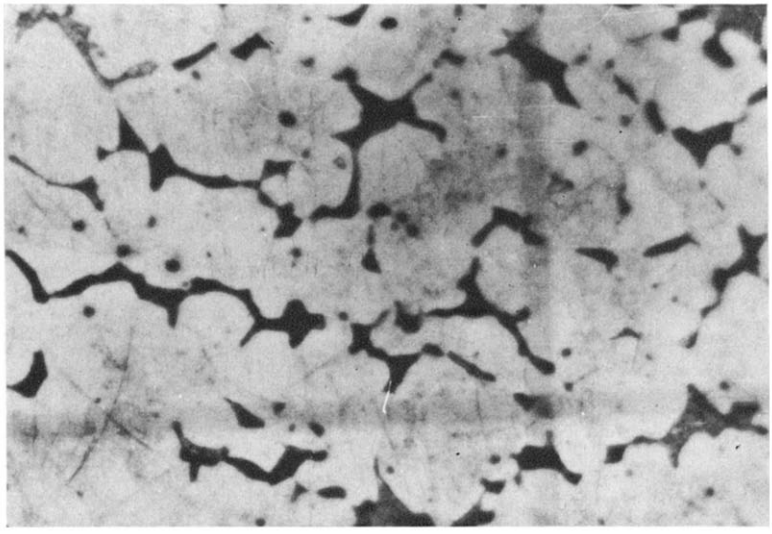

FIG. B.4. Yellow brass. × 250

FIG. B.5. Side of slug, yellow brass. ×250

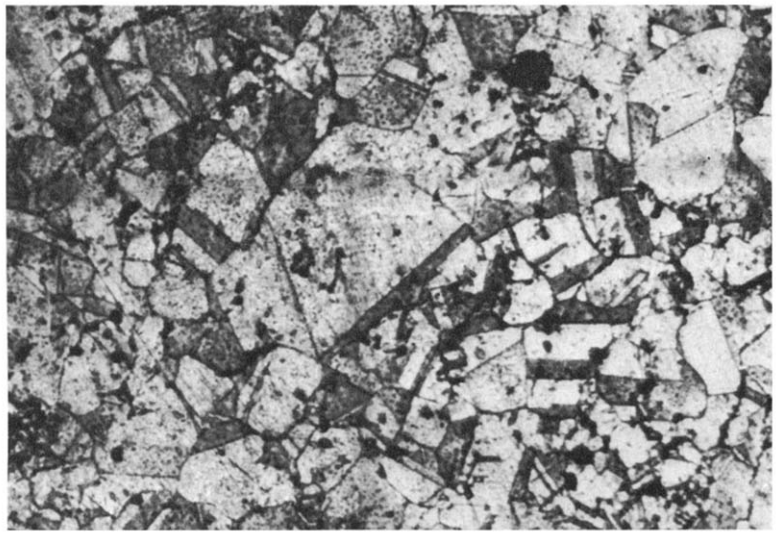

FIG. B.6. Copper. 250

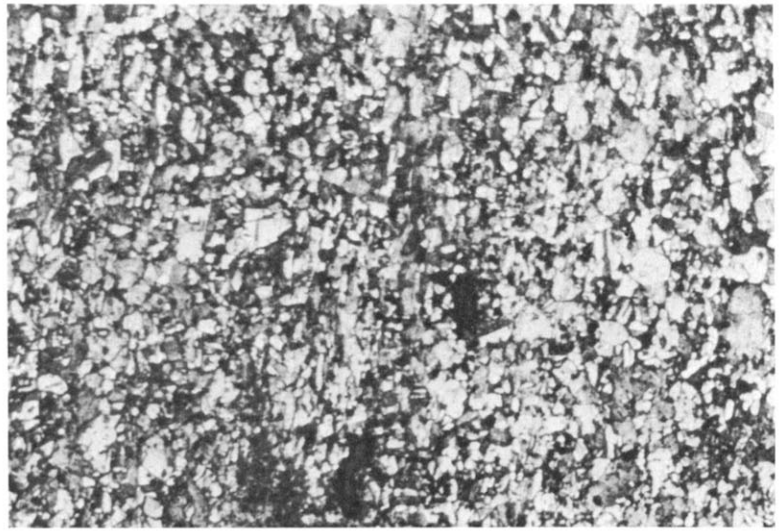

FIG. B.7. Copper slug. ×250

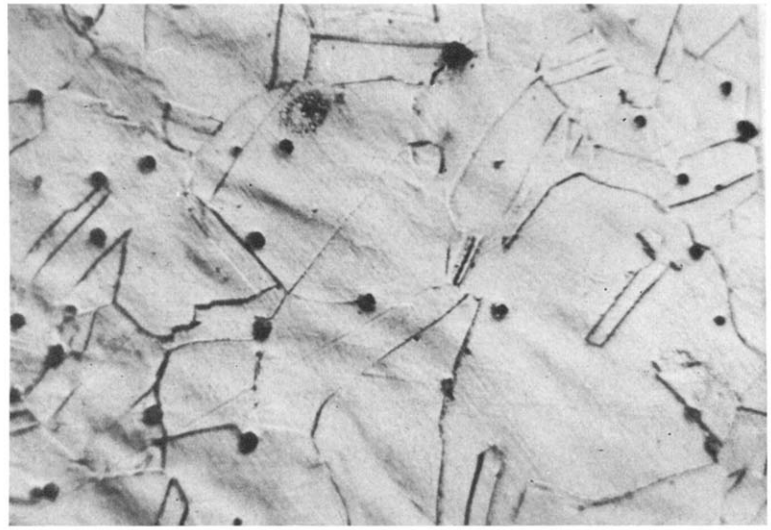

FIG. B.8. Monel. ×250

FIG. B.9. Monel slug, along the longitudinal axis. × 250

FIG. B.10. Center of the slug, monel. × 250

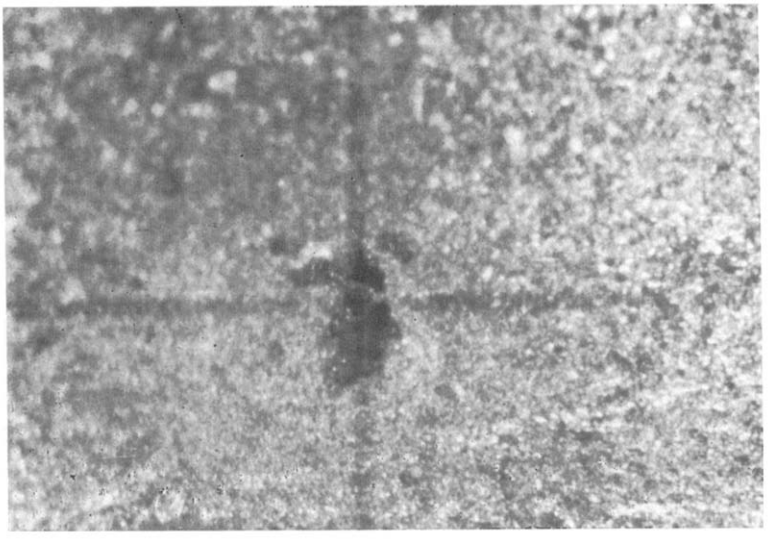

FIG. B.11. Monel slug along transverse axis. Recrystallization occurred near the center. ×250

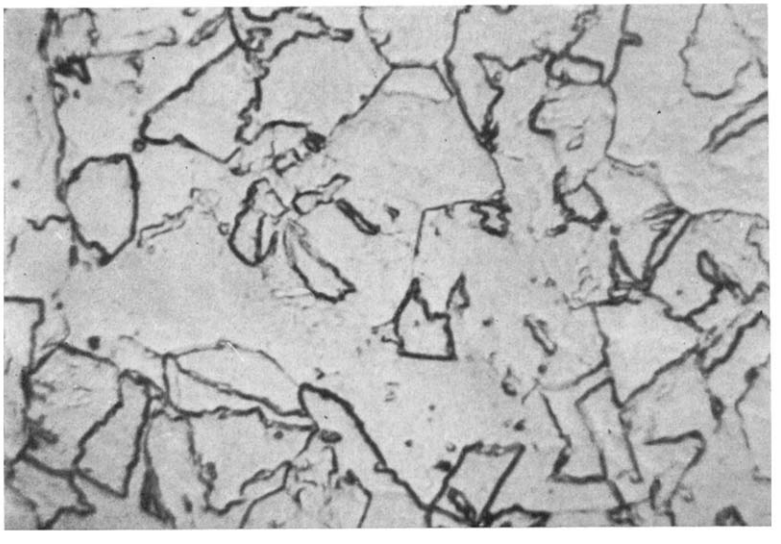

FIG. B.12. Maraging steel. ×250

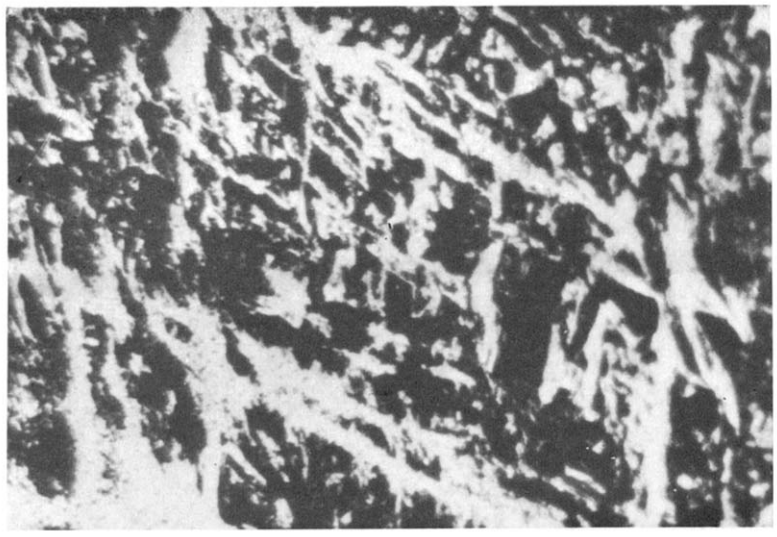

FIG. B.13. Maraging steel slug. 250

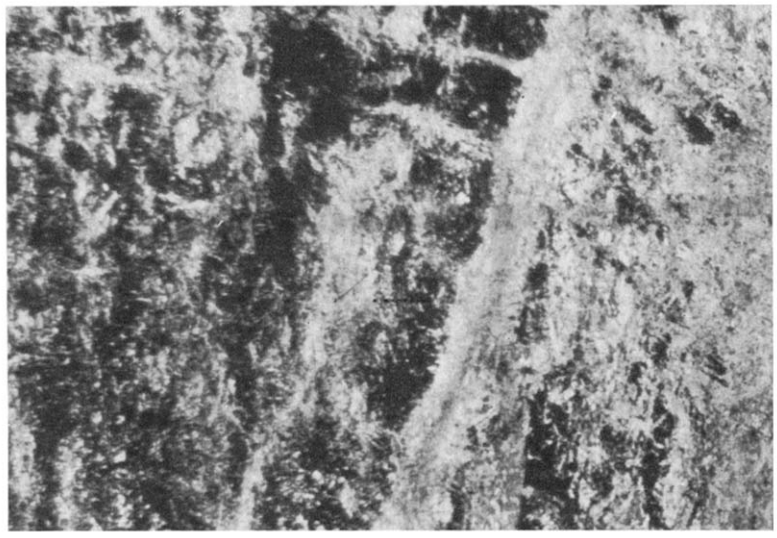

FIG. B.15. Maraging steel slug at edge. 250

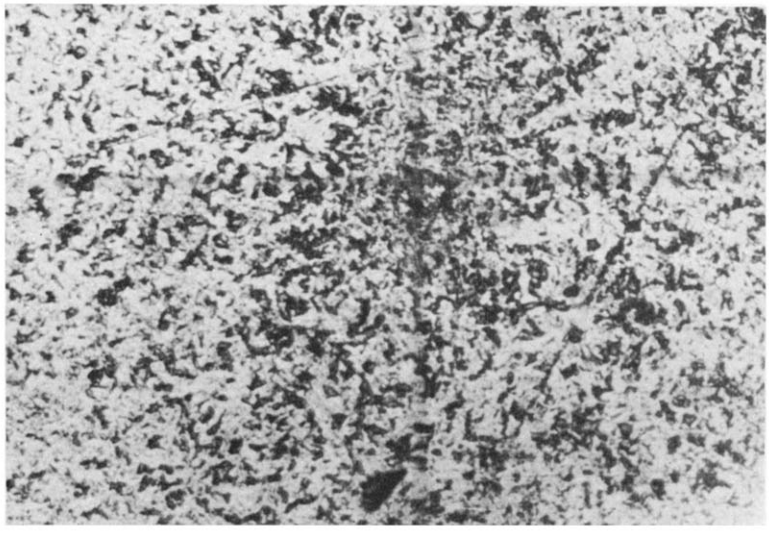

FIG. B.16. Maraging steel slug at center. ×250

gradiating up to 10 percent of the original metal grains (Fig. B.11). The hardness of the slug had increased from 12·5 RC to 21 RC.

Figures B.12 and B.13. Maraging steel (Vascomax 250). The grain boundaries are well defined and the grains are equiaxed. Annealing twins are visible. Figure B.13 was taken at the edge of the transverse axis of the slug. White lines are fractures while the black area is unidentified.

Figure B.14. A sketch of the steel slug showing variations in hardness. The outer edge of the metal was fractured. The fractures extend toward the center in a conical pattern.

Figures B.15 and B.16. The structure at the edge of the steel slug at the longitudinal axis and the center of the slug. No microstructure is visible at this magnification. Some phase transformation is suspected. The grains increase in size away from the center. The hardness of the slug had increased from 28·5 RC to 36·75 RC (average), suggesting some degree of precipitation.